

Vapour pressure deficit modulates hydraulic function and structure of tropical rainforests under nonlimiting soil water supply

Oliver Binks^{1,2} , Lucas A. Cernusak³ , Michael Liddell³ , Matt Bradford⁴, Ingrid Coughlin² , Callum Bryant² , Ana C. Palma³ , Luke Hoffmann³, Iftakharul Alam³, Hannah J. Carle² , Lucy Rowland⁵ , Rafael S. Oliveira⁶ , Susan G. W. Laurance³, Maurizio Mencuccini¹  and Patrick Meir^{2,7} 

¹CREAF, Cerdanyola del Vallès, Barcelona, 08193, Spain; ²Research School of Biology, The Australian National University, Canberra, 2601, ACT, Australia; ³Centre for Tropical Environmental and Sustainability Science, College of Science and Engineering, James Cook University, Cairns, 4878, Qld, Australia; ⁴CSIRO Land and Water, Atherton, 4883, Qld, Australia; ⁵Geography, Faculty of Environment Science and Economy, University of Exeter, Laver Building, Exeter, EX4 4QE, UK; ⁶Departamento de Biologia Vegetal, Instituto de Biologia, Universidade Estadual de Campinas (UNICAMP), Campinas, 13083-970, SP, Brazil; ⁷School of Geosciences, University of Edinburgh, Edinburgh, EH9 3FF, UK

Summary

Author for correspondence:
Oliver Binks
Email: ojbinks@gmail.com

Received: 28 March 2023
Accepted: 7 August 2023

New Phytologist (2023)
doi: 10.1111/nph.19257

Key words: allometry, canopy conductance, canopy-atmosphere coupling, drought stress, hydraulic vulnerability, rainforest hydraulics, tree height, vapour pressure deficit.

- Atmospheric conditions are expected to become warmer and drier in the future, but little is known about how evaporative demand influences forest structure and function independently from soil moisture availability, and how fast-response variables (such as canopy water potential and stomatal conductance) may mediate longer-term changes in forest structure and function in response to climate change.
- We used two tropical rainforest sites with different temperatures and vapour pressure deficits (VPD), but nonlimiting soil water supply, to assess the impact of evaporative demand on ecophysiological function and forest structure. Common species between sites allowed us to test the extent to which species composition, relative abundance and intraspecific variability contributed to site-level differences.
- The highest VPD site had lower midday canopy water potentials, canopy conductance (g_c), annual transpiration, forest stature, and biomass, while the transpiration rate was less sensitive to changes in VPD; it also had different height–diameter allometry (accounting for 51% of the difference in biomass between sites) and higher plot-level wood density.
- Our findings suggest that increases in VPD, even in the absence of soil water limitation, influence fast-response variables, such as canopy water potentials and g_c , potentially leading to longer-term changes in forest stature resulting in reductions in biomass.

Introduction

The flux of water from the terrestrial landscape to the atmosphere fundamentally influences the Earth's energy budget and hydrological cycle and is mediated by its pathway through vegetation. Over short timescales, vegetation controls water vapour fluxes by varying stomatal conductance, but over greater temporal and spatial scales, fluxes are determined by vegetation community composition, structure, biomass, and leaf area (Stegen *et al.*, 2011; Iio *et al.*, 2014; Schlesinger & Jasechko, 2014; Silvertown *et al.*, 2015; Wei *et al.*, 2017). Thus, changes in the supply and demand of water, that is the hydraulic environment, influence carbon assimilation and storage at the landscape scale (Law *et al.*, 2002; Tang *et al.*, 2014; Álvarez-Dávila *et al.*, 2017). In this study, we examine the interaction between short- and long-term feedbacks between the hydraulic environment and the land-atmosphere exchange of water and carbon in terms of transpiration, growth rates and

biomass; and the extent to which these processes are mediated by species composition and intraspecific variation, in two climatologically different tropical rainforests.

Characterising hydraulic traits relating to tree performance under drought conditions has become a research priority (Sperry & Love, 2015; Anderegg *et al.*, 2016) due to the reported increase in drought-induced tree mortality globally (Allen *et al.*, 2015; Hammond *et al.*, 2022). The traits shown to be most representative of species' responses to water stress are as follows: P50 – the water potential at 50% loss of hydraulic conductivity and the hydraulic safety margin; HSM – the difference between P50 and a minimum observed water potential (Choat *et al.*, 2012; Oliveira *et al.*, 2021). However, high levels of biodiversity, interactions among species, trait plasticity, and variation in species' relative abundance in time and space make it difficult to characterise the community-level hydraulic vulnerability of diverse systems such as tropical rainforests (Bittencourt *et al.*, 2020).

Community traits (i.e. community weighted trait means; Grime, 1998), are subject to environmental selection at three levels: (1) species composition due to environmental filtering (Kraft *et al.*, 2015; Duarte *et al.*, 2018), (2) species relative abundance (Martin & Canham, 2020), and (3) intraspecific variation (Gratani, 2014; Henn *et al.*, 2018; Monroe *et al.*, 2020). Where community traits differ systematically over environmental gradients (Ackerly & Cornwell, 2007), the three mechanisms above operate predominately at large, intermediate, and local scales, respectively. This pattern is consistent with spatial gradients of hydraulic traits, where there is a general trend from communities with high P50, small HSMs, and high leaf water potentials in regions of high water availability, to the opposite trait values in drier regions (Anderegg, 2015; Trugman *et al.*, 2020). Over large spatial scales, these differences predominantly reflect changes in species composition (Sanchez-Martinez *et al.*, 2020; J.M.R. Peters *et al.*, 2021), while at more local scales, intraspecific variability plays a stronger role (Rosas *et al.*, 2019).

High energy input and water availability result in the disproportionately large contribution of tropical rainforests to global budgets of carbon, water and energy, accounting for *c.* 25% of the carbon stored in the terrestrial biosphere (Bonan, 2008) and supplying *c.* 35% of terrestrial precipitation through transpired water (Schlesinger & Jasechko, 2014). Despite precipitation (> 1750 mm yr⁻¹; Moncrieff *et al.*, 2015) exceeding evapotranspiration (1000–1400 mm yr⁻¹; McJannet, 2007a; Baker *et al.*, 2021), tropical rainforests are nevertheless susceptible to drought-related declines in productivity (Gatti *et al.*, 2014; Hubau *et al.*, 2020) and transpiration (Zeri *et al.*, 2014; Mallick *et al.*, 2016), and increases in mortality (Phillips *et al.*, 2009, 2010). Moreover, differences in water availability over short distances within rainforests have been shown to cause significant variation in community-level hydraulic traits (Schiatti *et al.*, 2014; Cosme *et al.*, 2017; Barros *et al.*, 2019; Tavares *et al.*, 2023), illustrating the impact of the hydraulic environment on forest structure and species composition.

Relevant gradients in the hydraulic environment are not always related to precipitation or soil moisture (Novick *et al.*, 2016; Trueba *et al.*, 2017; Oliveira *et al.*, 2021). Strong theoretical grounds exist to suggest that vapour pressure deficit (VPD in kPa, or *D* as mole fraction; see Table 1 for descriptions of abbreviations) drives plant hydraulic traits resulting from feedbacks between stomatal conductance, leaf water potential, and transpiration (McDowell & Allen, 2015; Grossiord *et al.*, 2020; Fang *et al.*, 2021). Omitting the gravity component (which remains constant), the average leaf water potential (Ψ_{leaf}) relates to soil water potential (Ψ_{soil}), transpiration (E), plant hydraulic conductance (k), and canopy conductance (g_c) as: $\Psi_{\text{leaf}} = \Psi_{\text{soil}} - (E/k) = \Psi_{\text{soil}} - (D \cdot g_c)/k$ (Whitehead *et al.*, 1984). Therefore, while Ψ_{soil} forms the baseline (i.e. the intercept), VPD determines the magnitude and sensitivity of canopy water potentials to changing atmospheric conditions (i.e. the slope). Consequently, VPD is likely to have a direct impact on canopy water potentials, canopy conductance, and whole-plant hydraulic conductance (Olson *et al.*, 2020; Binks *et al.*, 2021). Additionally, because Ψ_{leaf} relates to turgor pressure within living cells, VPD may indirectly affect

Table 1 Description and units of abbreviations used in the text.

Abbreviations	Units/Constants	Description
CB	–	Cow Bay: field site with the highest VPD
RC	–	Robson Creek: field site with lowest VPD
VPD; <i>D</i>	kPa; unitless	Vapour pressure deficit; mole fraction vapour pressure deficit
$\Psi_{\text{leaf,soil,PD,MD}}$	MPa	Water potential. Subscripts represent leaf, soil, predawn leaf, and midday leaf, respectively
E	kg s ⁻¹ m ⁻²	Transpiration per one-sided leaf area
k	kg s ⁻¹ MPa ⁻¹ m ⁻²	Whole-plant hydraulic conductance per one-sided leaf area
g_s	kg s ⁻¹ m ⁻²	Stomatal conductance per one-sided leaf area
P50; P80	MPa	Water potential at 50% or 80% loss of hydraulic conductivity
HSM _{fd,Mod}	MPa	Hydraulic safety margin. The difference between the P50 and the minimum observed leaf water potential as measured in the field (subscript fd), or the minimum modelled water potential (subscript Mod).
DBH	m	Tree diameter at breast height
$J_s; J_{s_plot}$	kg cm ⁻¹ h ⁻¹ ; kg h ⁻¹ ha ⁻¹	Sap flux normalised by cm tree circumference; sap flux, or transpiration, per hectare
PAR	μmol m ⁻² s ⁻¹	Photosynthetically active radiation
PAD	%	Per cent air discharged
Temp	°C	Temperature
RGR	kg kg ⁻¹ yr ⁻¹	Relative growth rate
AGB	kg or kg ha ⁻¹	Aboveground biomass of a single tree (kg – used for deriving relative growth rate), or a whole plot (kg ha ⁻¹)
g_{av}	m s ⁻¹	Aerodynamic conductance to water vapour
g_c	m s ⁻¹	Canopy conductance to water vapour
ρ	1.183 kg m ⁻³	Density of air
c_p	1010 J kg ⁻¹ K ⁻¹	Specific heat capacity of air
γ	66 Pa K ⁻¹	Psychrometric constant
λ	2.442 × 10 ⁶ J kg ⁻¹	Heat of vaporisation of water

growth rate (Lockhart, 1965) and plant height (Woodruff *et al.*, 2004; Niklas, 2007; Potkay *et al.*, 2021). Thus, all else equal, one might expect forests growing under higher VPD to be more hydraulically resistant (e.g. have lower P50s), but have smaller stature and lower relative growth rates. However, while predicted increases in VPD (Zhang *et al.*, 2015) are expected to influence vegetation growth globally (Sanginés de Cárcer *et al.*, 2018; Yuan *et al.*, 2019; Bryant *et al.*, 2021), few ecological studies have addressed the relative impacts of VPD and soil water on community- or plot-level hydraulic traits (Grossiord *et al.*, 2020; Olson *et al.*, 2020; López *et al.*, 2021).

In this study, we make use of two climatically different tropical rainforest sites without soil water limitation (Binks *et al.*, 2021) to

test the impact of VPD combined with higher temperatures on forest structure, water stress (canopy water potentials), water use (transpiration), hydraulic traits ($P50$, HSM , g_c), relative growth rates, and tree allometry. Overlapping species composition between sites allows us to test the contribution of intraspecific variation compared with differences in community composition to site-level differences.

Thus, we have two main hypotheses: H1. We expect that the site with the highest VPD will have lower canopy water potentials, be more drought resistant (e.g. lower $P50$), have lower canopy conductance, lower growth rates, and have smaller stature. H2. Differences in emergent site-level hydraulic and structural traits will be attributable to both intraspecific variation (of overlapping species) and differences in species composition. In addition, we explore site-level drivers of transpiration, focusing on the possible coordination in the sensitivity of sap flux to soil water potential (supply) vs VPD (demand).

Materials and Methods

Study sites

The study was conducted at two seasonally wet tropical rainforest sites 100 km apart in northern Australia. Cow Bay (CB, 16.238S, 145.427E) is a wet lowland rainforest (elevation: 86 m) with a mean annual rainfall of 3700 mm (2008–2021 site data). The forest census plot at CB is 1 ha in size (50 m \times 200 m) with a stream winding through the length of the plot. The length and width of the stream were measured throughout the plot and deducted from the plot area to give a total forested area of 0.8 ha. Robson Creek (RC, lat. 17°121'S, long. 145°634'E) is an upland rainforest (elevation: 700 m) with a mean annual rainfall of 2264 mm (2011–2021 site data), consisting of a 25 ha plot, divided into 1 ha subplots. Both sites have acidic dystrophic brown dermosol soil, but at CB, the upper horizon comprises 33% sand, 55% silt, and 12% clay, whereas RC is 44–48% sand, 16–21% silt, and 35–36% clay. Both sites are strongly seasonal with *c.* 70% of rainfall occurring between January and April (Bradford *et al.*, 2014b). The sites have not been accessed by logging companies for over 50 yr, before which logging was minimal due to the presence of protected riparian habitat in both plots (personal communication with landowners; Bradford *et al.*, 2014a).

Cow Bay has significantly higher VPD and temperature than RC, but lower wind speed (Fig. 1; Table 2). Soil water content and rooting depth are similar at both sites, and previous work indicates that the fractional contribution of soil hydraulic resistance to the entire vertical hydraulic pathway is the same across sites at *c.* 10% in the dry season (Binks *et al.*, 2021). The two sites share 37 tree species, which account for 30.6 % of all trees (> 10 cm DBH) at CB, and 37.9 % of all trees at RC.

Species selection

Focal trees were selected for measurements of sap flux, hydraulic vulnerability curves, and leaf water potentials. Nine species were selected, of which seven occur at CB, six occur at RC, and four occur at both sites ('overlapping species', Table 3). Focal trees were

selected such that each species was represented by a size range from 12–22 cm to > 30 cm diameter at breast height (DBH).

At CB, the focal species account for 10.7% of all trees and 18.5% of the total biomass; of which the overlapping species account for 3.3% of all trees and 4.2% of the biomass in the plot. At RC, the focal species account for 21.6% of all trees and 15.3% of the total biomass; of which the overlapping species account for 16.3% of all trees and 12.4% of the biomass.

Meteorological measurements and soil water potential

Both sites have meteorological towers measuring air temperature and relative humidity (Rotronics HC2S3 or Vaisalla HMP45A), precipitation (Rimco RIM-8000; Campbell Scientific, Garbur, Qld, Australia), photosynthetically active radiation (PAR, Li-190; Li-Cor Biosciences, Lincoln, NE, USA), net radiation (NR01; Hukseflux, Delft, the Netherlands), 3D wind speed (CSAT3 sonic anemometer; Campbell Scientific), and infrared gas analysers for measuring CO₂ and H₂O concentrations, (Li7500 or Li7500A depending on year and site, Li-Cor Biosciences). In CB, the tower is located in the corner of the plot and is *c.* 5 m taller than the upper canopy height, while in RC, the tower is located *c.* 300 m from the focal plot used in this study and is > 10 m above the upper canopy. Both sites have structurally heterogeneous canopies, *c.* 25 m tall, with no emergent trees.

Soil water potential (Ψ_s) was measured at both sites (Supporting Information Fig. S1) using Teros 21 matric potential sensors (Meter Group, Pullman, WA, USA). Sensors were installed at depths 0.1, 0.5, 1.0, and 2.0 m below ground level where possible, in 75 mm boreholes, at four locations at RC and three locations at CB. Data loggers were constructed from Arduino Uno microcontrollers (www.Arduino.cc) with Adafruit data logger shields (www.adafruit.com). More detailed information on the installation and loggers can be found in Binks *et al.* (2021).

Sap flux (J_s)

Sap flux sensors (EMS81; Environmental Monitoring Systems, Brno, Czech Republic) logging at 15-min intervals were installed on the south side of the focal trees at both sites (Table 3). The EMS81 sensors use the heat balance method, heating a relatively large volume of tissue spanning the whole depth of the xylem. Consequently, it is not necessary to calculate sapwood depth, or radial sap flux profiles, and the sap flux value is in units normalised by circumference, kg cm⁻¹ h⁻¹. Sensor installation occurred over a period of months, but a full year of data was obtained for comparison of the two sites from June 2019 for CB and March 2019 for RC.

The meteorological conditions during the period of sap flux measurement did not deviate substantially from the long-term average conditions of VPD, air temperature, and wind speed (Fig. S2). The water content of the soil surface did appear to drop to lower than normal levels in CB over the last half of the measurement period (Fig. S2); however, the soil matric potential of the top 2 m of soil was more negative at RC than at CB over the same period (Fig. S1). The trees at both sites have been shown to primarily acquire water from between 1 and 2 m depth (Binks *et al.*, 2021).

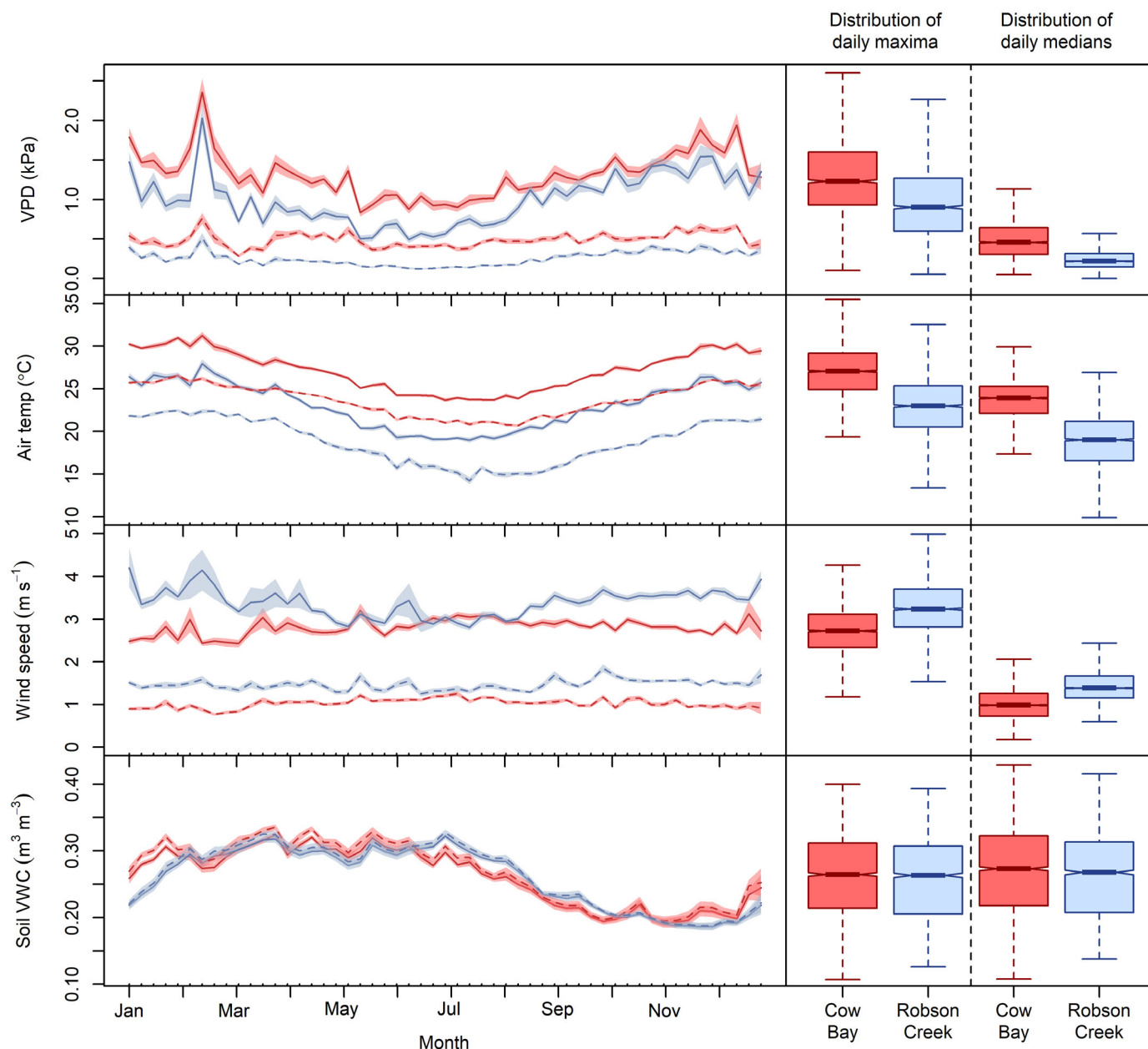


Fig. 1 Climate comparison between Robson Creek (RC, blue) and Cow Bay (CB, red) from multiyear datasets (8 yr for CB and 10 yr for RC), where soil VWC is the soil volumetric water content. Lines in the panels on the left connect points, each of which represents a weekly mean of the daily maximum (solid lines) and daily median (dashed lines). The shaded areas indicate one standard error of the mean, and the number of days per point ranges from a minimum of 44 to a maximum of 77. The small dashes on the x-axis are the weekly points at which the data were averaged. The boxplot shows the distribution of the daily maxima and medians. Boxplot interpretation: the bold line represents the median value, the box is the interquartile range, and the whiskers extend to either 1.5 times the interquartile range or to the most extreme data point, depending on which is closest to the median; the notch corresponds to the 95% confidence interval of the median.

Baselining J_s data

Initial baseline values of J_s were taken when (1) VPD < 0.1 kPa continuously for 2 h, (2) J_s during the same period was at the daily minimum, and (3) that the standard deviation of J_s during the same 2-h period was less than the mean (i.e. J_s was stable; Oishi *et al.*, 2016; Ward *et al.*, 2017). When mean J_s between the hours of 04:00 h and 06:00 h, was lower than either of the adjacent (before or after) baseline values, then these lower J_s were

added as additional baseline points. Baseline values were then connected, providing a value for each time point, using linear interpolation and subtracted from measured J_s .

Gap filling

Gaps in the sap flux data, due to power or sensor failure, were filled using autoregressive models (da Costa *et al.*, 2017). In brief, power-transformed J_s data were linearly regressed against air

Table 2 Comparison of the annual mean and standard errors of the daily maxima and median meteorological conditions between Robson Creek (RC) and Cow Bay (CB), where 'VPD' is vapour pressure deficit and 'VWC soil' is the volumetric water content of the soil surface.

	Long-term conditions				P value	Conditions over duration of study				
	RC		CB			RC		CB		P value
	Mean	SE	Mean	SE		Mean	SE	Mean	SE	
VPD (kPa)										
Max.	1.008	0.012	1.330	0.013	< 0.001	1.050	0.028	1.621	0.031	< 0.001
Median	0.257	0.004	0.493	0.005	< 0.001	0.282	0.008	0.507	0.010	< 0.001
Air temp. (°C)										
Max.	23.056	0.065	27.211	0.050	< 0.001	22.733	0.161	28.754	0.124	< 0.001
Median	18.756	0.058	23.733	0.037	< 0.001	18.394	0.140	23.887	0.090	< 0.001
Wind speed (m s⁻¹)										
Max.	3.383	0.025	2.812	0.015	< 0.001	3.321	0.030	2.925	0.044	< 0.001
Median	1.467	0.009	1.029	0.007	< 0.001	1.550	0.019	0.993	0.015	< 0.001
VWC soil (m³ m⁻³)										
Min.	0.259	0.001	0.260	0.001	< 0.001	0.269	0.003	0.251	0.002	< 0.001
Median	0.264	0.001	0.268	0.001	0.019	0.274	0.003	0.259	0.003	< 0.001

Long-term conditions are based on 7 yr of data from RC and 10 yr from CB, while the 'Conditions over duration of study' occurred during the period over which sap flux sensors were installed. The probability values are derived from a two-way, unpaired Student's *t*-test.

Table 3 Number of trees per site and species.

Species	Family	No. of trees per site		No. of trees per species
		Robson Creek	Cow Bay	
<i>Dysoxylum papuanum</i>	Meliaceae	4	0	4
<i>Endiandra microneura</i>	Lauraceae	3	0	3
<i>Myristica globosa</i> subsp. <i>muelleri</i>	Myristicaceae	4	0	4
<i>Argyrodendron peralatum</i>	Sterculiaceae	4	4	8
<i>Cardwellia sublimis</i>	Proteaceae	2	4	6
<i>Cryptocarya mackinnoniana</i>	Lauraceae	2	4	6
<i>Litsea leefeana</i>	Lauraceae	4	4	8
<i>Daphnandra repandula</i>	Monimiaceae	0	4	4
<i>Sloanea australis</i> subsp. <i>parviflora</i>	Elaeocarpaceae	0	4	4
	Total	23	24	47

temperature, PAR, VPD, Ψ_{soil} and against the preceding 6 h of values for J_s in order to remove the autoregressive component of the data. The resulting models explained over 90% of the variance in sap flux from all trees in RC, and all except one tree in CB ($r^2 = 0.74$). The median amount of gap-filled data per tree was 3.5%; however, one tree at CB was removed due to having 50% of its data missing.

Predawn and midday leaf water potentials

Predawn and midday leaf water potentials (Ψ_{PD} and Ψ_{MD}) were measured in three field campaigns with the intention of capturing

peak dry (November 2019), intermediate (September 2019), and wet (March 2020) seasons. A small terminal branch containing a minimum of four leaves was collected from each tree using rope access and pole pruners to obtain the upper-most (and sunlit for Ψ_{MD}) leaves. Leaves, stored in sealed humidified bags, were measured for water potential with a Scholander pressure chamber (PMS Instruments Co., Albany, OR, USA) from 1 to 3 h after collection, where each tree was represented by at least three leaves. Samples for Ψ_{PD} were collected between 04:30 h and 06:30 h, and samples for Ψ_{MD} were collected between 12:30 h and 14:30 h.

Pneumatic branch vulnerability curves

A single branch 1.5–2.5 m length was collected from the upper canopy of each focal tree (Table 3) before 10:00 h from each site and immediately placed in water and double bagged. The samples were then transported to the laboratory (*c.* 2.5 h away) and left to rehydrate overnight.

The process consisted of taking a series of measurements of stem air content while the branch dried down to -10 MPa, which was the limit of the pressure chamber (Pereira *et al.*, 2016; Bittencourt *et al.*, 2018). Following a period of dry down and subsequent equilibration (1 h or more), branch water potential was measured from three leaves, after which the 'scars' from leaf removal were sealed using PVA glue. Air was then sucked out of the stem into a reservoir, initially at sub-atmospheric pressure (40 kPa), enabling calculation of the per cent air discharged (PAD) and subsequent inference of the per cent loss of conductivity (Fig. S3). The pneumatic method has been rigorously compared with other methods for determining hydraulic vulnerability and found to provide nonbiased estimates of P50 (Zhang *et al.*, 2018; Sergent *et al.*, 2020; Zhao *et al.*, 2023). Refer to Methods S1 for further detail.

Per cent air discharged data were analysed using the R package 'FITPLC' (Duursma & Choat, 2017), which fits a Weibull distribution to the PAD data, and uses bootstrapping to determine the leaf water potential at 50% and 80% air discharge, with 95% confidence (CI) intervals. These values were used as proxies for P50 and P80, while P50 was also used with dry season midday water potentials to calculate the hydraulic safety margin, $HSM = \Psi_{MD} - P50$.

Upscaling J_s to plot

Midday values of sap flux were found not to vary systematically by species or by DBH at either site (reported by Binks *et al.*, 2021). As J_s was expressed per circumference in the sensor output ($\text{kg cm}^{-1} \text{h}^{-1}$), it was scaled to plot level (J_{s_plot} , kg h^{-1}) by multiplying the median value of J_s by the sum of the circumference of all trees on the plot. To estimate the variance of the J_{s_plot} value, however, a bootstrapped median was based on 1000 repetitions from which 95% CI were extracted using the R package BOOT (Canty & Ripley, 2022).

Environmental drivers of midday J_{s_plot}

A comparison was made of the main environmental drivers of midday (12:00 h–14:00 h) J_{s_plot} across sites and seasons using a regression of the form $J_{s_plot} \sim VPD + \text{Temp} + \text{PAR} + \Psi_{soil} + \text{Wind speed}$, similar to the gap-filling protocol. The analysis was performed on the whole year of data from each site, and on the driest and wettest month to determine seasonal changes. To avoid multicollinearity arising from including all soil depths in the model, Ψ_{soil} from the depth with the highest positive Pearson r , from the correlation $J_{s_plot} \sim \Psi_{soil}$, was selected as the single Ψ_{soil} depth to be included in the model.

Despite the risk of variance inflation arising as a consequence of including both temperature and VPD in the models, it was considered important to represent temperature in the models due to the temperature difference between sites (Fig. 1). For RC, the maximum variance inflation factors were < 5 , while for CB they were all < 8 .

Comparing J_s between plots

To directly compare the transpiration of both sites under standard conditions, J_{s_plot} (continuous data, not midday values) from each site was empirically modelled using PAR, VPD, and air temperature (Ψ_{soil} did not vary enough diurnally to be included in this model). The models were then used to predict the transpiration of both sites under standard conditions, that is the 'average day' in the driest month in CB; that is, the half-hourly averaged conditions of November 2020. For each time point, a random normal distribution of 1000 values was generated from the J_{s_plot} model outputs based on the error terms associated with the model coefficients; where the error represents the variance of the median sap flux over the repeated cycles of VPD, temperature, and PAR. Thus, each modelled output had a distribution of values enabling a statistical comparison of sites over the

'standard day'. Hysteresis (accounting for the lag in response between J_s and meteorological drivers due to water storage) was not considered within the model, as the added complexity and associated error were considered unnecessary to determine whether there was a difference between sites.

Statistics

The variables measured in this study (Ψ_{PD} , Ψ_{MD} , P50, P80, and HSM) were analysed using linear regression models, and significance was estimated using type III ANOVAs to avoid the sequential analysis of predictor variables. Following Binks *et al.* (2021), two model structures were used to ensure the effects of species composition and intraspecific variation (encompassing phenotypic plasticity and/or genotypic variation) were adequately accounted for: $y \sim \text{Site:Sp}$, testing solely for site differences in the overlapping species; and $y \sim \text{Site} + \text{Sp} + \text{DBH} + \text{Site} : \text{DBH} + \text{Sp} : \text{DBH}$, testing for all other interactions – note the only missing interaction in this second model is Site:Sp. These model structures were used to test P50, P80 and HSM. As leaf water potentials are responses rather than traits, they were only tested per season for differences between Site and Sp.

All variables were tested for normality and were subsequently log, or power transformed where necessary using the boxcox function in R to find the optimal power. The variables were transformed for analysis as follows: $\log(\text{P50})$, $\log(\text{P80})$, HSM , $\Psi_{PD}^{0.55}$, and $\Psi_{MD}^{0.95}$.

Comparing allometry, tree size, and growth between sites

Comparisons of tree height and DBH, the allometric relationship between DBH and height, and relative growth rate were all based on inventory data taken in 2012 and 2018 at CB, and 2010 and 2019 at RC.

Tree height was measured in the inventory data for 2012 at CB and 2010 at RC, enabling the fitting of site-specific allometric relationships between DBH and tree height as per Feldpausch *et al.* (2012): $\text{Height} = a(1 - \exp(-b \cdot \text{DBH}^c))$, using nonlinear least squares (nls) regression. All inventory data (excluding palms, lianas, and ferns) were used from each site to test for allometric differences, resulting in there being more data from Robson Creek (25 ha, $n = 23\,311$) than Cow Bay (1 ha, $n = 488$). However, data from each site were confined to a standard range of DBH (10–90 cm), and the regression diagnostic plots suggested the model residuals were normally distributed around the estimate. Comparisons were based on (1) all species at both sites, and (2) only species occurring at both sites (hereafter 'overlapping species'). Site-level differences were tested for significance by comparing two nonlinear models that included and excluded 'site' as a factor using ANOVA.

The contribution of intraspecific variation to site-level differences in overlapping species was determined as the Site:Sp interaction in linear models of the form $x \sim \text{Site} \times \text{Sp}$ where 'x' represents tree Height, DBH, or the allometric relationship between Height and DBH.

Relative growth rate (RGR) was determined by scaling DBH to whole-tree aboveground biomass $AGB = 0.0673 (WD \cdot DBH^2 \cdot Height)^{0.976}$, where WD is wood density (Chave *et al.*, 2014) and using change in biomass over the census interval $(t_1 - t_0)$, where $RGR = \log_c(AGB_{t_1}) - \ln(AGB_{t_0}) / (t_1 - t_0)$ (Pommerening & Muszta, 2016). Species-level wood density data were acquired from a CSIRO database (Murphy *et al.*, 2013; Bradford & Murphy, 2019). The estimate of AGB at RC was compared using the DBH-height relationship derived from CB to test whether allometric differences between sites result in differences in AGB.

Linear regression models were used to test the relationships between RGR, Site, and Species. As there was no Site \times Species interaction, the final model structure was $RGR \sim Site + Species$.

Canopy conductance, g_c

Canopy conductance (g_c) was determined for each site using the long-term data sets as per Tan *et al.* (2019): $\frac{1}{g_c} = \frac{\rho C_p VPD}{\gamma \lambda E} + \left(\frac{\Delta H}{\gamma \lambda E} - 1 \right) \left(\frac{1}{g_{av}} \right)$, where ρ and C_p are the density and specific heat capacity of air, respectively, Δ is the slope of the saturation vapour pressure–temperature relationship, H is the sensible heat flux, γ is the psychrometric constant, and λE is the latent heat flux measured from the flux tower (Table 1). g_{av} is the aerodynamic conductance to water vapour, which was calculated following Binks *et al.* (2020). Days with rainfall were excluded from the analysis to increase the extent to which calculated g_c represents canopy-level stomatal conductance, and not evaporation of intercepted rainfall (McJannet, 2007b; Binks

et al., 2020). To make a seasonal comparison, we used data from the driest and wettest month (November and July, respectively) from each site, and took an aggregated median g_c per 1-h time increment. The data, between the hours of 08:00 h and 18:00 h, were then compared between sites using a paired Student t -test.

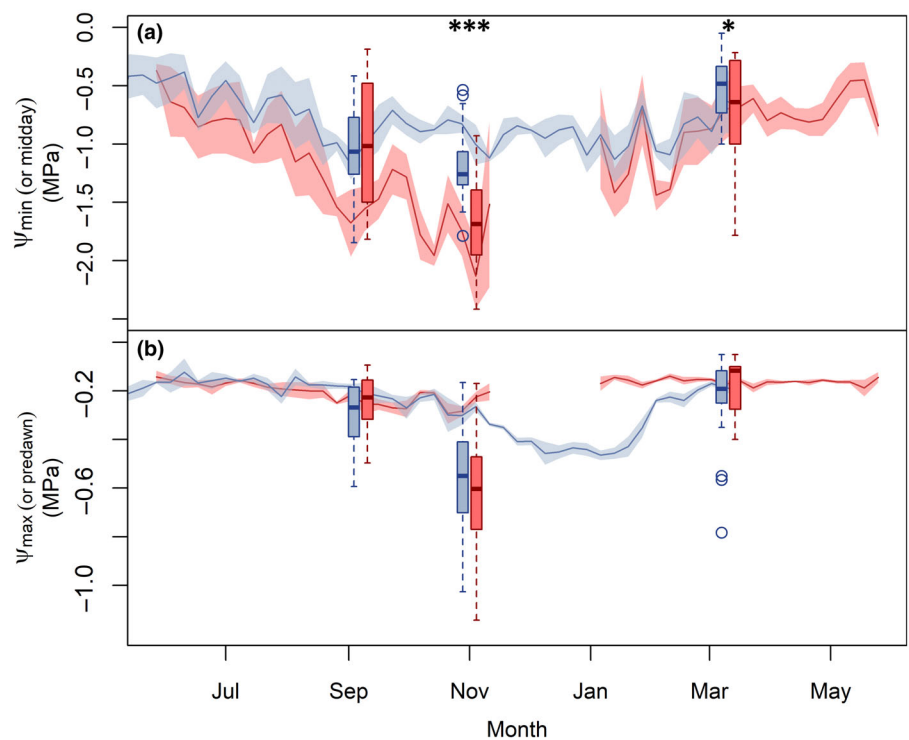
Calculating continuous canopy water potentials

Whole-tree hydraulic conductance (k_{tree}) was calculated using sap flux, soil water potential and canopy water potentials as per Binks *et al.* (2021), and continuous canopy water potentials were then calculated as: $\Psi_{canopy} = \Psi_{soil} - 0.01 \text{ Height} - (J_s / k_{tree})$, (Fig. S4). Because k_{tree} was found to change seasonally at CB (Binks *et al.*, 2021), k_{tree} was calculated three times a year (when leaf water potential data were collected) and then assumed to change linearly between time points.

During the wet season, all soil layers become wet and converge on the maximum sensor value (Fig. S1). Consequently, where data were missing in the wet season, the value at 2 m depth was taken as the mean value of sensors at the other soil depths. In the dry season, however, this assumption could not be made, and we therefore chose not to fill this gap in CB data in the dry season (Fig. 2).

Modelled water potentials were also used to derive hydraulic safety margins (HSM_{mod}), providing the opportunity to assess the difference in HSM based on water potential estimates outside of the field measurement period. This estimate was calculated for each site using the mean of bootstrapped values of $P50_{tree} - \Psi_{min_i}$ where Ψ_{min_i} was generated from a normal distribution ($n = \text{number of } P50_{tree} \text{ values}$) based on the modelled $\Psi_{min} \pm SD$.

Fig. 2 Canopy water potentials (Ψ) over the course of 1 yr at Robson Creek (RC) and Cow Bay (CB). The boxes (red CB, blue RC) represent field measurements of midday Ψ (a) and predawn Ψ (b), where significance, as determined by linear models and type 3 ANOVAs, is denoted by asterisks (*, $P < 0.05$; ***, $P < 0.001$). Lines (red CB, blue RC) are modelled values where each point represents the weekly mean value of daily canopy Ψ minima (upper panel) and maxima (lower panel) ± 1 SD. The gap in the CB data is due to sensor failure. Boxplot interpretation: the bold line represents the median value, the box is the interquartile range, and the whiskers extend to either 1.5 times the interquartile range or to the most extreme data point, depending on which is closest to the median. Values outside the whiskers are shown as open points.



Results

H1: Site-level differences in canopy water potentials, hydraulic traits, canopy conductance, stature, and growth rates, and H2: the community-level drivers of the differences

Midday leaf water potentials were significantly lower at CB than RC in dry season ($P < 0.001$, CB median, first and third quartiles: -1.69 MPa, -1.95 , -1.40 . RC: -1.26 MPa, -1.35 , -1.07), and in the wet season ($P = 0.043$, CB: -0.64 MPa, -0.98 , -0.31 . RC: -0.48 MPa, -0.70 , -0.34 ; Fig. 2, Table 4). Predawn water potentials (Ψ_{PD}) differ seasonally at both sites, but do not differ between sites across the seasons.

The P50 values estimated from the pneumatic method, and the hydraulic safety margins (HSM) showed no differences between sites or species, no intraspecific variation, and no relationship with DBH (Table 4). However, the estimated marginal mean P50 was more negative at CB (-3.66 MPa, 95% CI: -4.15 to -3.22) than at RC (-3.17 MPa, 95% CI: -3.57 to -2.81). HSMs were derived both from the minimum measured midday water potential field data (HSM_{fd}) and from modelled minimum canopy water potentials (HSM_{mod} , Fig. 2), where neither were significantly different between sites, but HSM_{fd} (mean \pm SE: 2.26 ± 0.14 MPa) was significantly larger than HSM_{mod} (1.76 ± 0.14 MPa, Fig. S5). This was presumably due to more negative water potentials occurring outside of the field measurement period.

Both sites showed seasonal variation in daytime g_c , where values were lower (but less variable) in the dry season (Fig. 3). RC had significantly higher daytime g_c between the hours of 08:00 h and 18:00 h in both seasons (dry season $P = 0.019$, wet season $P < 0.001$).

Table 4 Probability values representing significance based on a type III ANOVA of linear regressions where Ψ is water potential, P50 is the Ψ at 50% air discharge, hydraulic safety margins (HSM) is the difference between the minimum recorded midday Ψ and the P50, and DBH is the tree diameter at breast height.

Factor/Variable	Predawn Ψ	Midday Ψ	P50	HSM
Intraspecific variability	NT	NT	0.333	0.925
Site	0.592	0.02	0.131	0.627
Species	< 0.001	< 0.001	0.351	0.402
DBH	NT	NT	0.156	0.095
Season	< 0.001	< 0.001	NT	NT
Site:Season	0.23	0.006	NT	NT
Species:Season	NT	NT	NT	NT
Species:DBH	NT	NT	0.160	0.255
Site:DBH	NT	NT	–	0.475

'Site' is the site-level difference including species that do not occur at both sites; 'Species' is the difference between species accounting for site-level variance; and 'Intraspecific variation' is the inter-site difference between species that occur at both sites. The leaf water potentials here are from only the dry season. 'Intraspecific variation' was analysed in a separate model as denoted by the double underline. 'NT' indicates variables that were not tested in the original model, while a dash represents variables that were included in the initial model but were removed from the final model in response to step AIC analysis.

Values in bold are significant at $P < 0.05$.

The allometric relationships between tree height and DBH are significantly different between sites ($P < 0.001$, Fig. 4). In the comparison of all species at both sites, parameters b (initial slope) and c (shape parameter) were significantly different (Fig. 4a); while in overlapping species, all parameters (a (height), b , and c) were significantly different (Fig. 4b). There was a significant Site:Species interaction in the allometry ($P = 0.021$), and for the absolute values of height and DBH ($P < 0.001$ for both), suggesting the role of intraspecific variation. However, the total explained variance for this interaction was minimal at < 0.5 , 0.7 , and 0.9% for the allometry, height, and $\log(\text{DBH})$, respectively. The direct comparison of height and $\log(\text{DBH})$ revealed that trees at RC are taller (median values: RC 17.0 m, CB 15.0 m); and across all species, trees at RC had a smaller DBH (Fig. 5, median values: RC 16.3 cm, CB 17.4 cm). However, there was no difference in the median DBH of overlapping species between sites.

There were no site-level differences in relative growth rate ($P = 0.1737$).

Cow Bay had lower biomass (390 Mg ha^{-1}) than RC (451 Mg ha^{-1}). Using the height allometric equation derived for CB on the DBH data from RC, the estimate of RC biomass becomes 420 Mg ha^{-1} , suggesting that differences in allometry account for 51% of the difference in biomass between sites. Despite the higher biomass at RC, the median biomass of trees from overlapping species was significantly higher at CB (Fig. 5, $P = 0.042$). This is due to the higher estimated median wood density at that site ($P < 0.001$), which is also higher amongst overlapping species at CB ($P = 0.005$) due to there being fewer trees from lower wood density species in this group. Therefore, the higher overall biomass at RC can be attributed to a larger basal area at that site (RC = $44.8 \text{ cm}^2_{\text{tree}} \text{ m}^{-2}_{\text{ground_area}}$, CB = $39.0 \text{ cm}^2 \text{ m}^{-2}$) and taller trees.

Site-level drivers of transpiration: VPD vs soil water potential

Midday sap flux, throughout the whole year, was less sensitive to variations in VPD at CB than at RC (r^2 of 0.29 and 0.35, respectively; Table 5; Fig. 6), but soil water potential accounted for a greater proportion of the variance in CB than RC (r^2 of 0.13 and 0.06, respectively). However, this did not result in a significant difference in the diurnal plot-level transpiration compared under standard/reference conditions (Fig. 7).

Seasonally, VPD accounted for around a third of the variance in midday J_{s_plot} and air temperature accounted for $c. 1$ quarter at both sites (Table 5). The contribution of PAR varied between sites, and in CB, it accounted for more of the variance in the dry (0.32) than in the wet season (0.24); whereas in RC, it accounted for more of the variance in the wet (0.37) than in the dry season (0.23). Soil water potential accounted for little of the variance during the driest and wettest months, probably indicating that this parameter varies too slowly to influence sap flux within a single month.

The scaled annual transpiration at both sites seemed to be quite low compared with other rainforest sites (Kumagai *et al.*, 2005; Fisher *et al.*, 2007; Kunert *et al.*, 2017; Lion

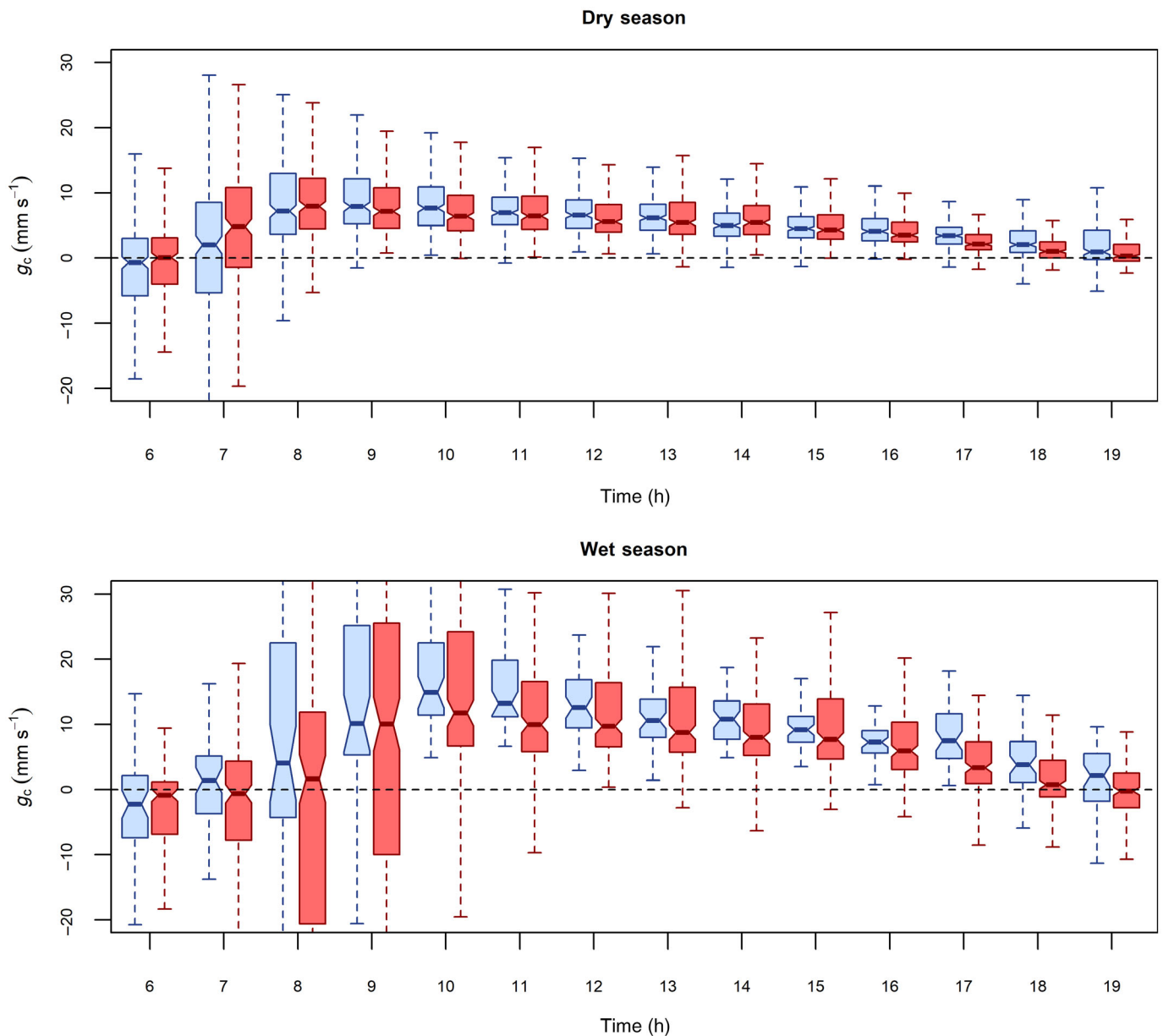


Fig. 3 Comparison of the diurnal cycle of canopy conductance between Cow Bay (CB, red boxes) and Robson Creek (RC, blue boxes) in the driest month (November) and wettest month (July). Each box represents the data recorded for each hour time interval over a 7 yr (RC) and 10 yr (CB) time series within the month of interest. RC has significantly higher g_c than CB in both the dry season ($P = 0.019$) and the wet season ($P < 0.001$) between the hours of 08:00 h and 18:00 h, as determined by a paired Student's t -test. The range on the y-axis was chosen to most clearly indicate the daytime trend in canopy conductance and, as a result, some of the ranges are not included in the plot. Boxplot interpretation: the bold line represents the median value, the box is the interquartile range, and the whiskers extend to either 1.5 times the interquartile range or to the most extreme data point, depending on which is closest to the median; the notch approximately corresponds to the 95% confidence interval of the median.

et al., 2017) at 372.4 mm (171.2–512.8, 95 % CI) for CB and 408.1 mm (171.6–536.7) for RC (Table 6). This estimate was based on a median flux from all of the trees because of the non-normal distribution of J_s values on which the scaling was based. Most studies, however, use regressions to scale J_s by DBH, assuming the J_s data across trees have a normal distribution. Our estimates increase if we scale by means rather than medians, resulting in values of 467.2 mm (277.4–642.8) for CB, and 585.6 mm (373.4–770.1) for RC, which are closer to previous estimates of transpiration from Australian tropical rainforests

(McJannet, 2007a). Both sites transpired more in the dry season than in the wet season (Table 6).

Discussion

The environment influences ecosystem function at different temporal scales. These range from the immediate impact of prevailing conditions on fast-response variables, such as canopy water potential, to the medium-term impact, for example, of plant water potential on growth rates, to the longer-term effects of

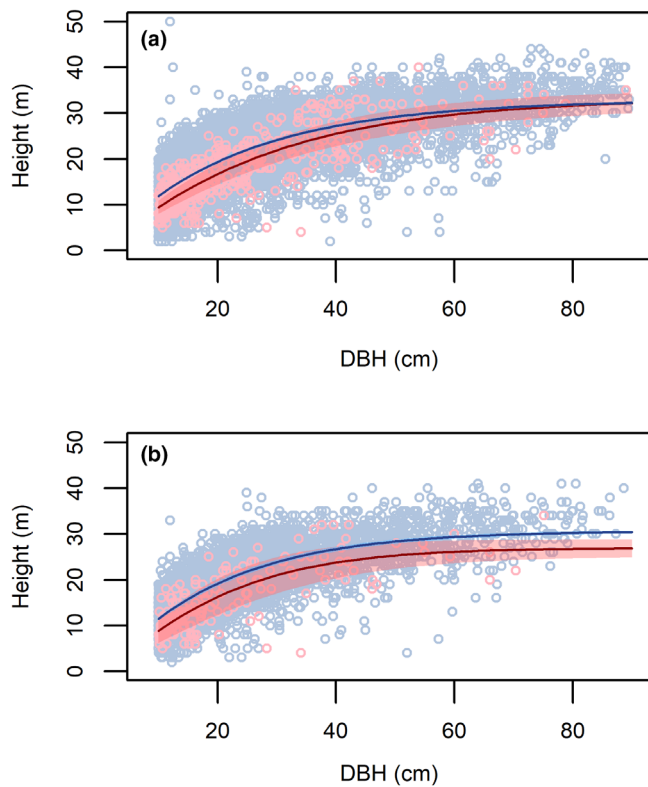


Fig. 4 Allometric relationships between height and the diameter at breast height (DBH) (a) of all individuals from all species on both sites, and (b) from only the species that occur at both sites. Curves represent the allometric equation derived by Feldpausch *et al.* (2012) of the form: $\text{height} = a(1 - \exp(-b \cdot \text{DBH}^c))$, fitted using nonlinear least squares regression with standard deviation. Blue points and line represent Robson Creek, while red points and line represent Cow Bay. The areas shaded in blue (Robson Creek, difficult to see) and red (Cow Bay) represent the 95% confidence intervals of the predicted relationships. There is a significant difference ($P < 0.001$) between site-level allometry in both analyses.

species selection. Here we aimed to assess the role of VPD in shaping site-level differences at short to medium-temporal scales, and the extent to which intra- and interspecific variability (longer-term) contributed to these differences.

Are the forests at each site ecophysiologicaly different (H1)?

Differences in dry and wet season midday canopy water potentials (Fig. 2) suggest that the forests at each site do indeed experience different levels of water stress, while a lack of difference in predawn water potentials between sites throughout the year is consistent with there being minimal (or at least equal) soil water limitation. The lower daytime canopy conductance at CB (Fig. 3) probably accounts for the lower estimated annual transpiration (Table 6) at that site, despite the higher VPD and temperature (Fig. 1). This raises the question of whether the lower g_c at CB is a direct mechanistic response to higher VPD and/or lower Ψ_{canopy} (meaning that both sites would behave identically under the same conditions), or if the forests differ physiologically, that is are adapted, to different conditions. The analysis of the

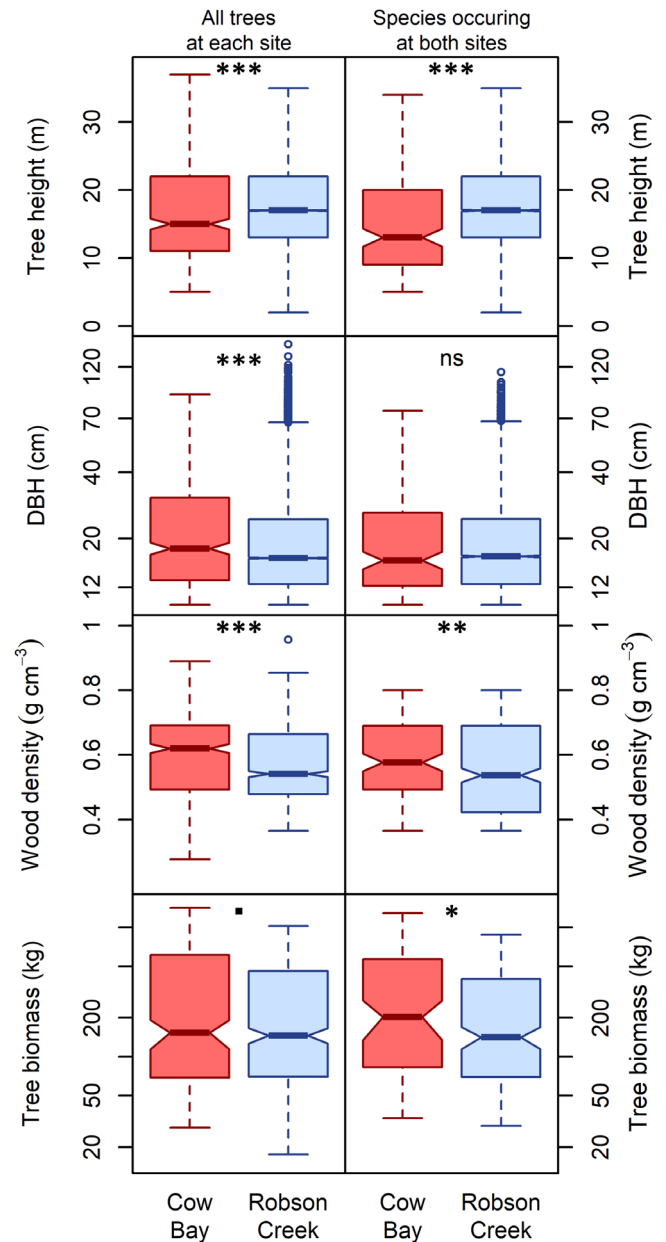


Fig. 5 Comparison between Robson Creek (RC) and Cow Bay (CB) of trees > 10 cm diameter at breast height (DBH) of: Tree height, DBH, species-specific wood density, and aboveground tree biomass. The panels on the left include all trees at both sites, while panels on the right only include trees from the species that occur at both sites, (CB red, RC blue). The asterisks represent the probability of a significant difference between boxes: ***, < 0.001 ; **, < 0.01 ; *, < 0.05 ; •, < 0.10 ; ns, not significant. DBH and tree biomass data are log transformed. Boxplot interpretation: the bold line represents the median value, the box is the interquartile range, and the whiskers extend to either 1.5 times the interquartile range or to the most extreme data point, depending on which is closest to the median; the notch approximately corresponds to the 95% confidence interval of the median. Values outside the whiskers are shown as open points.

sap flux drivers indicates the latter, where transpiration in the forest at CB (higher VPD) is less sensitive to VPD (Fig. 6; Table 5). This is consistent with a modelled trend indicating that under identical conditions the forest at CB would transpire less; however, the difference in that case was not significant (Fig. 7).

Table 5 Proportion of variance in midday (12:00 h–14:00 h) sap flux explained by environmental drivers; seasons represent data from the driest and wettest months.

Season Site	Wet		Dry		Whole year	
	RC	CB	RC	CB	RC	CB
Drivers						
VPD	0.31	0.36	0.31	0.29	0.35	0.29
Temp	0.23	0.25	0.24	0.22	0.04	0.09
PAR	0.31	0.22	0.20	0.32	0.35	0.27
Soil Ψ	0.02 ²	0.02 ²	0.08 ¹	0.06 ^{0.5}	0.06 ²	0.13 ¹
Wind speed	0.08	0.10	0.11	0.00	0.06	0.04
Highest VIF	VPD: 4.8	Temp: 7.4	VPD: 4.6	Temp: 7.7	VPD: 2.4	VPD: 4.6
Model r^2	0.94	0.95	0.92	0.86	0.85	0.82

Models were not simplified from the starting structure to facilitate comparison between sites and seasons. The models contained a value for soil water potential (soil Ψ) from a single soil depth represented by the subscript, for example 0.02² is the r^2 value for 2 m depth. Soil depths were selected on the basis of having the highest Pearson correlation coefficient in a direct comparison with the sap flux data. Because temperature (Temp) and vapour pressure deficit (VPD) are closely related, variance inflation was tested, and the highest variance inflation factor (VIF) from each of the models, with the associated variable, is represented in the table. The variable initials and symbols are as follows: PAR, photosynthetically active radiation; soil Ψ , soil water potential; VPD, vapour pressure deficit; while RC and CB are the field sites Robson Creek and Cow Bay, respectively.

Structurally, there were differences in site-level wood density (Fig. 5) and in allometry, where trees from CB tend to be shorter for a given DBH (Fig. 4), and are shorter in general (Fig. 5). Cyclones occur with reasonably high frequency along the Australian tropical northeast coastline in the wider region of CB, which could contribute to the reduced height of trees at that site through damage to the upper tree crowns (Terry *et al.*, 2022). However, the last major cyclone in the CB region occurred in 1999 (Murphy *et al.*, 2013), and no cyclone damage has been reported in the locality of CB since then. Moreover, in general, CB has lower recorded average wind speeds, lower maximum wind speeds (Fig. 1), and had fewer events where wind speed exceeded 15 m s⁻¹ over the measurement period (8 yr for CB

and 10 yr for RC). Thus, it seems unlikely that the allometric or height differences are caused by cyclones, or at least exclusively by cyclones, especially given the high growth rate of tropical trees, that is typically twice the rate of temperate trees (Locosselli *et al.*, 2020).

The focal species at each site did not appear to differ in terms of hydraulic resistance to water stress (P50 – here estimated using the pneumatic method) or in the hydraulic safety margin (Table 4; Fig. S5), in contrast to other studies showing clear differences in these parameters over larger gradients of water availability (Rosas *et al.*, 2019; J.M.R. Peters *et al.*, 2021). Therefore, to address hypothesis 1, the main differences between sites appeared to be the physiological regulation of canopy conductance (Fig. 3); the structural differences associated with allometry (Fig. 4), wood density, and tree size (Fig. 5); and the species composition and relative abundance.

The contribution of intraspecific variation and species composition to site-level differences (H2)

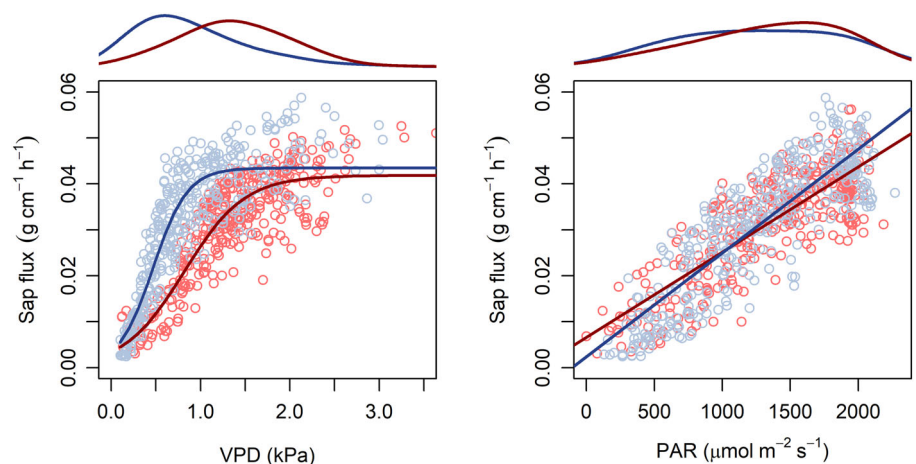
Intraspecific variation (relating to phenotypic plasticity and/or differences in genotype) was found to contribute significantly to site-level differences in allometry, height, and DBH, but only accounted for a minimal fraction of the total variance between sites (all < 1%). Our analysis of wood density was based on species' mean values in the region, rather than being measured at each site, and therefore, our study was unable to test for intraspecific variation within this parameter. Consequently, the structural differences between sites (tree allometry, height, DBH, and wood density) detected in this study were principally attributed to species composition and relative abundance.

Canopy water potentials and sap flux differed between sites, but intraspecific cross-site variability was not analysed for these fast-response variables because of their dependence on the immediate conditions.

Ecophysiological acclimation to different VPD regimes

Hydraulic vulnerability in trees is inherently difficult to characterise (Jansen *et al.*, 2015). The lack of significant difference

Fig. 6 Comparison of the relationships of vapour pressure deficit (VPD) and photosynthetically active radiation (PAR) with midday sap flux (J_s) across sites, where each point represents an average value between 12:00 h and 14:00 h in a single day for a single tree. Density plots show the frequency distribution of VPD and PAR at each site during the study period. Points and lines in blue represent Robson Creek, while the points and line in red represent Cow Bay. There is a sigmoidal fit between J_s and VPD of the form $J_s = a/(1 + \exp((b - \text{VPD})/c))$, and a linear fit between J_s and PAR.



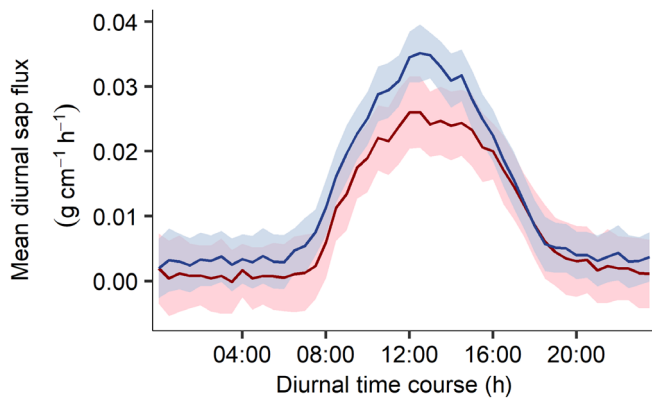


Fig. 7 Comparison of the modelled sap flux (J_s) of Cow Bay (CB, red) and Robson Creek (RC, blue) over the course of an ‘average’ day of the driest month at CB. The mean of the vapour pressure deficit (VPD), photosynthetically active radiation (PAR) and wind speed (W_s) was found for each half-hour interval over the course of November 2020 – soil water potential was not used because it does not change substantially over the course of a day. These conditions were then used to drive the model $J_s \sim \text{VPD} + \text{PAR} + W_s$, which was applied to data from each site. Thus, the output is the predicted transpiration of each site under standard conditions where the shaded areas represent the standard error of the estimate.

Table 6 Plot-level transpiration (E) with 95% confidence intervals (CI).

	Robson Creek		Cow Bay	
	E	95% CI	E	95% CI
Annual (mm yr^{-1})	408.1	171.6–536.7	372.4	171.2–512.8
Dry season (mm d^{-1})	1.3	0.6–1.6	1.1	0.3–1.4
Wet season (mm d^{-1})	1	0.3–1.5	0.9	0.3–1.4

Seasonal values of transpiration are the daily median value taken from the driest and wettest months.

detected in P50s between sites may be partly due to variation between individuals, noise generated through the measurement procedure, and the species-level sample sizes (Bittencourt *et al.*, 2020). Indeed, the (nonsignificant) difference in plot-level marginal mean P50s ($P=0.131$) suggests that there may have been a significant difference if sample sizes were bigger, or measurement-related noise was less. Previous research indicates that RC and CB have different whole-tree- and site-level hydraulic conductance (Binks *et al.*, 2021), confirming the different selection pressures of the hydraulic environment at each site. However, hydraulic conductance has been shown to be a labile trait in several studies (Schuldt *et al.*, 2011; Tng *et al.*, 2018), while P50 is known to be taxonomically conservative (Rowland *et al.*, 2023). It is possible that P50 and HSM principally respond to soil water availability, while whole-tree hydraulic conductance is more sensitive to evaporative demand: perhaps as a result of turgor-driven differences in growth (Kroeger *et al.*, 2011), vessel size (Hacke *et al.*, 2001; R.L. Peters *et al.*, 2021), and leaf area.

Leaf water potential plays a central role in mediating stomatal conductance (Brodribb *et al.*, 2003; Brodribb & Holbrook, 2003; Klein, 2014; Bartlett *et al.*, 2016; Tsuji *et al.*, 2020), and species

and communities in higher VPD environments tend to have stomatal conductance with lower sensitivity to changes in VPD (Oren *et al.*, 1999; Klein, 2014), and lower gross ecosystem productivity (Novick *et al.*, 2016; Grossiord *et al.*, 2020; Smith *et al.*, 2020). Stomatal sensitivity can also be coordinated with hydraulic conductance, where species that respond more quickly to changes in VPD have higher hydraulic conductance (Tsuji *et al.*, 2020). The findings from this and our previous study are consistent with both of these conclusions, where transpiration at the highest VPD site (CB) had the lowest sensitivity to changes in VPD (Fig. 6), and had lower whole-tree hydraulic conductance (Binks *et al.*, 2021). The more negative values of minimum canopy water potentials at CB (Fig. 2) may cause the lower absolute values of canopy conductance at that site (Fig. 3).

Acknowledging the possible contribution of cyclone damage between sites, there is significant theoretical and empirical evidence linking the hydraulic environment to tree height. Water stress is predicted to result in shorter trees by biophysical models that account for height-related impacts of water stress on physiology (Niklas, 2007; Olson *et al.*, 2018; Liu *et al.*, 2019), and by empirical allometric models describing height–diameter relationships over climate gradients (Lines *et al.*, 2012; Fu *et al.*, 2016; Fortin *et al.*, 2019; Zhang *et al.*, 2019). Turgor limitation places constraints on vertical growth in particular (Potkay *et al.*, 2021), providing a biophysical explanation for the different allometries between sites: This difference in tree structure accounts for 51% of the difference in biomass between sites.

Central to the ecophysiological response is the role of turgor pressure on vessel size (R.L. Peters *et al.*, 2021), stomatal conductance (Buckley, 2019), and growth (Potkay *et al.*, 2021). For a given water potential, osmotic potential determines turgor pressure, where osmotic adjustment is known to be a common response to water stress (Rada *et al.*, 1985; Bartlett *et al.*, 2014; Binks *et al.*, 2016). We did not measure leaf water relations in this study, so we cannot rule out that site-level differences in water potential were compensated for by differences in osmotic potential and not turgor pressure. However, taken together, the ecophysiological differences between sites (canopy conductance, wood density, and height) are consistent with those arising due to lower turgor pressures at CB.

VPD and rainforest biomass

The findings of this study show that the forest at CB experiences greater levels of canopy water stress than RC, and this impacts canopy conductance and probably accounts for the structural differences that lead to lower biomass. CB has over 1400 mm yr^{-1} more rainfall, similar soil moisture, and a higher dry season soil water potential; therefore, the lower plant water potentials are caused by higher levels of VPD. The difference in biomass between the sites is driven by differences in basal area and allometry and is not compensated for by the higher community-level wood density at the higher VPD site. Therefore, the lower height at CB is consistent with theoretical and empirical evidence linking canopy height with evaporative demand. The structural differences between forests were largely due to species composition,

indicating a strong role of environmental filtering in determining forest structure. However, intraspecific variation was significant, suggesting the potential for structural plasticity in the response of forests to future changes in VPD and temperature, resulting in gradual changes in biomass over time.

We speculate that in the short term (i.e. within the lifetime of a tree), increases in VPD may result in a reduction of canopy height caused by, for example, reduced growth or the loss of upper branches (Anfodillo & Olson, 2021), due to the increased water stress experienced by the upper canopy. Over time, existing species with higher wood density, lower hydraulic conductance and smaller stature may increase in relative abundance. Over longer time scales still, species composition may alter to favour species that are more competitive given the prevailing environmental constraints.

Conclusion

The results of this study suggest that the lower canopy water potentials at CB, arising as a consequence of higher evaporative demand and lower whole-tree hydraulic conductance, affect a cascade of physiological responses influencing gas exchange, tree allometry, plot-level wood density, and ultimately biomass. The ecophysiological differences between sites appear to over-compensate for the higher VPD at CB resulting in lower annual transpiration at that site. A plausible mechanistic interpretation is that lower water potentials result in turgor pressure-related reductions in vertical growth and average cell size, resulting in shorter trees, with lower hydraulic conductivity and higher wood density. Contrary to expectation, our results did not reveal a significant difference in the hydraulic vulnerability (P50, HSM) between sites (Gleason *et al.*, 2015). Our research indicates that sustained increases in VPD will probably result in shorter-stature tropical rainforests with associated reductions in rainforest biomass.

Acknowledgements

This work was supported by ARC grant DP17010409 to PM; Catalan science and technology grant, Beatriu de Pinós, BP2021 00224 to OB. OB gratefully acknowledges the Daintree Discovery Centre for the use of their facilities and power supply for the field equipment. ML acknowledges the support of TERN in maintaining the field infrastructure at Cow Bay and Robson Creek, TERN is the Australian Government's Terrestrial Ecosystem Research Network (www.tern.org.au). Open access publishing facilitated by Australian National University, as part of the Wiley - Australian National University agreement via the Council of Australian University Librarians.

Competing interests

None declared.

Author contributions

OB led and implemented the study, wrote the paper with PM, MM, LAC, RSO, LR, SL and ML and analysed the data with IC,

HJC and MM. ML and MB contributed data and provided equipment. IC, CB, ACP, LH, IA and OB collected field data.

ORCID

Oliver Binks  <https://orcid.org/0000-0002-6291-3644>
 Callum Bryant  <https://orcid.org/0000-0002-8035-9157>
 Hannah J. Carle  <https://orcid.org/0000-0003-2893-6081>
 Lucas A. Cernusak  <https://orcid.org/0000-0002-7575-5526>
 Ingrid Coughlin  <https://orcid.org/0000-0002-8541-2682>
 Michael Liddell  <https://orcid.org/0000-0001-9754-8184>
 Patrick Meir  <https://orcid.org/0000-0002-2362-0398>
 Maurizio Mencuccini  <https://orcid.org/0000-0003-0840-1477>
 Rafael S. Oliveira  <https://orcid.org/0000-0002-6392-2526>
 Ana C. Palma  <https://orcid.org/0000-0003-2083-3037>
 Lucy Rowland  <https://orcid.org/0000-0002-0774-3216>

Data availability

All data are available from the Terrestrial Ecosystem Research Network (TERN) Data Portal: <https://portal.tern.org.au/metadata/TERN/db33762b-1199-4dbd-b151-b6ce8d5ad042>. doi: <https://doi.org/10.25901/86yk-5m77>.

References

- Ackerly DD, Cornwell WK. 2007. A trait-based approach to community assembly: partitioning of species trait values into within- and among-community components. *Ecology Letters* 10: 135–145.
- Allen CD, Breshears DD, McDowell NG. 2015. On underestimation of global vulnerability to tree mortality and forest die-off from hotter drought in the Anthropocene. *Ecosphere* 6: art129.
- Álvarez-Dávila E, Cayuela L, González-Caro S, Aldana AM, Stevenson PR, Phillips O, Cogollo Á, Peñuela MC, Von Hildebrand P, Jiménez E *et al.* 2017. Forest biomass density across large climate gradients in northern South America is related to water availability but not with temperature. *PLoS ONE* 12: 1–16.
- Anderegg WRL. 2015. Spatial and temporal variation in plant hydraulic traits and their relevance for climate change impacts on vegetation. *New Phytologist* 205: 1008–1014.
- Anderegg WRL, Klein T, Bartlett M, Sack L, Pellegrini AFAA, Choat B, Jansen S. 2016. Meta-analysis reveals that hydraulic traits explain cross-species patterns of drought-induced tree mortality across the globe. *Proceedings of the National Academy of Sciences, USA* 113: 5024–5029.
- Anfodillo T, Olson ME. 2021. Tree mortality: testing the link between drought, embolism vulnerability, and xylem conduit diameter remains a priority. *Frontiers in Forests and Global Change* 4: 704670.
- Baker JCA, Garcia-Carreras L, Gloor M, Marsham JH, Buermann W, Da Rocha HR, Nobre AD, De Carioca AA, Spracklen DV. 2021. Evapotranspiration in the Amazon: spatial patterns, seasonality, and recent trends in observations, reanalysis, and climate models. *Hydrology and Earth System Sciences* 25: 2279–2300.
- Barros F, Bittencourt PRL, Brum M, Restrepo-Coupe N, Pereira L, Teodoro GS, Saleska SR, Borma LS, Christoffersen BO, Penha D *et al.* 2019. Hydraulic traits explain differential responses of Amazonian forests to the 2015 El Niño-induced drought. *New Phytologist* 223: 1253–1266.
- Bartlett MK, Zhang Y, Kreidler N, Sun S, Ardy R, Cao K, Sack L. 2014. Global analysis of plasticity in turgor loss point, a key drought tolerance trait. *Ecology Letters* 17: 1580–1590.
- Bartlett MK, Klein T, Jansen S, Choat B, Sack L, Bartlett MK, Klein T, Jansen S, Choat B, Sack L. 2016. The correlations and sequence of plant stomatal,

- hydraulic, and wilting responses to drought. *Proceedings of the National Academy of Sciences, USA* 113: 13098–13103.
- Binks O, Cernusak LA, Liddell M, Bradford M, Coughlin I, Carle H, Bryant C, Dunn E, Oliveira R, Mencuccini M *et al.* 2021. Forest system hydraulic conductance: partitioning tree and soil components. *New Phytologist* 233: 1667–1681.
- Binks O, Finnigan J, Coughlin I, Disney M, Calders K, Burt A, Vicari MB, da Costa AL, Mencuccini M, Meir P *et al.* 2020. Canopy wetness in the Eastern Amazon. *Agricultural and Forest Meteorology* 297: 108250.
- Binks O, Meir P, Rowland L, da Costa AC, Vasconcelos S, de Oliveira AR, Ferreira L, Christoffersen B, Nardini A, Mencuccini M. 2016. Plasticity in leaf-level water relations of tropical rainforest trees in response to experimental drought. *New Phytologist* 211: 477–488.
- Bittencourt PRL, Oliveira RS, da Costa ACL, Giles AL, Coughlin I, Costa PB, Bartholomew DC, Ferreira LV, Vasconcelos SS, Barros FV *et al.* 2020. Amazonia trees have limited capacity to acclimate plant hydraulic properties in response to long-term drought. *Global Change Biology* 26: 3569–3584.
- Bittencourt PRL, Pereira L, Oliveira RS. 2018. Pneumatic method to measure plant xylem embolism. *Bio-Protocol* 8: e3059.
- Bonan GB. 2008. Forests and climate change: forcings, feedbacks, and the climate benefits of forests. *Science* 320: 1444–1449.
- Bradford M, Murphy HT. 2019. The importance of large-diameter trees in the wet tropical rainforests of Australia. *PLoS ONE* 14: 1–16.
- Bradford MG, Metcalfe DJ, Ford A, Liddell MJ, McKeown A. 2014a. Floristics, stand structure and aboveground biomass of a 25-ha rainforest plot in the wet tropics of Australia. *Journal of Tropical Forest Science* 26: 543–553.
- Bradford MG, Murphy HT, Ford AJ, Hogan DL, Metcalfe DJ. 2014b. Long-term stem inventory data from tropical rain forest plots in Australia. *Ecology* 95: 2362.
- Brodribb TJ, Holbrook NM. 2003. Stomatal closure during leaf dehydration, correlation with other leaf physiological traits 1. *Plant Physiology* 132: 2166–2173.
- Brodribb TJ, Holbrook NM, Edwards EJ, Gutiérrez MV. 2003. Relations between stomatal closure, leaf turgor and xylem vulnerability in eight tropical dry forest trees. *Plant, Cell & Environment* 26: 443–450.
- Bryant C, Fuenzalida TI, Brothers N, Mencuccini M, Sack L, Binks O, Ball MC. 2021. Shifting access to pools of shoot water sustains gas exchange and increases stem hydraulic safety during seasonal atmospheric drought. *Plant, Cell & Environment* 44: 2898–2911.
- Buckley TN. 2019. How do stomata respond to water status? *New Phytologist* 224: 21–36.
- Canty A, Ripley B. 2022. Bootstrap functions (Originally by Angelo Canty for S) [R package boot v.1.3-28.1]. [WWW document] URL <https://CRAN.R-project.org/package=boot> [accessed 15 March 2023].
- Chave J, Réjou-Méchain M, Búrquez A, Chidumayo E, Colgan MS, Delitti WBC, Duque A, Eid T, Fearnside PM, Goodman RC *et al.* 2014. Improved allometric models to estimate the aboveground biomass of tropical trees. *Global Change Biology* 20: 3177–3190.
- Choat B, Jansen S, Brodribb TJ, Cochard H, Delzon S, Bhaskar R, Bucci SJ, Feild TS, Gleason SM, Hacke UG *et al.* 2012. Global convergence in the vulnerability of forests to drought. *Nature* 491: 752–755.
- Cosme LHM, Schiatti J, Costa FRC, Oliveira RS. 2017. The importance of hydraulic architecture to the distribution patterns of trees in a central Amazonian forest. *New Phytologist* 215: 113–125.
- da Costa AC, Rowland L, Oliveira RS, Oliveira AR, Binks OJ, Salmon Y, Vasconcelos S, Junior JA, Ferreira LV, Poyatos R *et al.* 2017. Stand dynamics modulate water cycling and mortality risk in droughted tropical forest. *Global Change Biology* 24: 1–10.
- Duarte LDS, Debastiani VJ, Carlucci MB, Diniz-Filho JAF. 2018. Analyzing community-weighted trait means across environmental gradients: should phylogeny stay or should it go? *Ecology* 99: 385–398.
- Duursma R, Choat B. 2017. FITPLC – an R package to fit hydraulic vulnerability curves. *Journal of Plant Hydraulics* 4: e002.
- Fang Y, Leung LR, Wolfe BT, Detto M, Knox RG, McDowell NG, Grossiord C, Xu C, Christoffersen BO, Gentine P *et al.* 2021. Disentangling the effects of vapor pressure deficit and soil water availability on canopy conductance in a seasonal tropical forest during the 2015 El Niño drought. *Journal of Geophysical Research: Atmospheres* 126: 1–20.
- Feldpausch TR, Lloyd J, Lewis SL, Brienen RJWW, Gloor M, Mendoza AM, Monteagudo Mendoza A, Lopez-Gonzalez G, Banin L, Abu Salim K *et al.* 2012. Tree height integrated into pantropical forest biomass estimates. *Biogeosciences* 9: 3381–3403.
- Fisher RA, Williams M, da Costa AL, Malhi Y, Da Costa RF, Almeida S, Meir P. 2007. The response of an Eastern Amazonian rain forest to drought stress: results and modelling analyses from a throughfall exclusion experiment. *Global Change Biology* 13: 2361–2378.
- Fortin M, Van Couwenberghe R, Perez V, Piedallu C. 2019. Evidence of climate effects on the height-diameter relationships of tree species. *Annals of Forest Science* 76: 1–20.
- Fu L, Sun W, Wang G. 2016. A climate-sensitive aboveground biomass model for three larch species in northeastern and northern China. *Trees* 31: 557–573.
- Gatti LV, Gloor M, Miller JB, Doughty CE, Malhi Y, Domingues LG, Basso LS, Martinewski A, Correia CSCC, Borges VF *et al.* 2014. Drought sensitivity of Amazonian carbon balance revealed by atmospheric measurements. *Nature* 506: 76–80.
- Gleason SM, Westoby M, Jansen S, Choat B, Hacke UG, Pratt RB, Bhaskar R, Brodribb TJ, Bucci SJ, Cao KF *et al.* 2015. Weak tradeoff between xylem safety and xylem-specific hydraulic efficiency across the world's woody plant species. *New Phytologist* 209: 123–136.
- Gratani L. 2014. Plant phenotypic plasticity in response to environmental factors. *Advances in Botany* 2014: 1–17.
- Grime JP. 1998. Benefits of plant diversity to ecosystems: immediate, filter and founder effects. *Journal of Ecology* 86: 902–910.
- Grossiord C, Buckley TN, Cernusak LA, Novick KA, Poulter B, Siegwolf RTW, Sperry JS, McDowell NG. 2020. Plant responses to rising vapor pressure deficit. *New Phytologist* 226: 1550–1566.
- Hacke UG, Sperry JS, Pockman WT, Davis SD, McCulloh KA. 2001. Trends in wood density and structure are linked to prevention of xylem implosion by negative pressure. *Oecologia* 126: 457–461.
- Hammond WM, Williams AP, Abatzoglou JT, Adams HD, Klein T, López R, Sáenz-Romero C, Hartmann H, Breshears DD, Allen CD. 2022. Global field observations of tree die-off reveal hotter-drought fingerprint for Earth's forests. *Nature Communications* 13: 1761.
- Henn JJ, Buzzard V, Enquist BJ, Halbritter AH, Klanderud K, Maitner BS, Michaletz ST, Pötsch C, Seltzer L, Telford RJ *et al.* 2018. Intraspecific trait variation and phenotypic plasticity mediate alpine plant species response to climate change. *Frontiers in Plant Science* 871: 1–11.
- Hubau W, Lewis SL, Phillips OL, Affum-Baffoe K, Beekman H, Cuní-Sanchez A, Daniels AK, Ewango CEN, Fauset S, Mukinzi JM *et al.* 2020. Asynchronous carbon sink saturation in African and Amazonian tropical forests. *Nature* 27: 80–87.
- Iio A, Hikosaka K, Anten NPR, Nakagawa Y, Ito A. 2014. Global dependence of field-observed leaf area index in woody species on climate: a systematic review. *Global Ecology and Biogeography* 23: 274–285.
- Jansen S, Schuldt B, Choat B. 2015. Current controversies and challenges in applying plant hydraulic techniques. *New Phytologist* 205: 961–964.
- Klein T. 2014. The variability of stomatal sensitivity to leaf water potential across tree species indicates a continuum between isohydric and anisohydric behaviours. *Functional Ecology* 28: 1313–1320.
- Kraft NJB, Adler PB, Godoy O, James EC, Fuller S, Levine JM. 2015. Community assembly, coexistence and the environmental filtering metaphor. *Functional Ecology* 29: 592–599.
- Kroeger JH, Zerkour R, Geitmann A. 2011. Regulator or driving force? The role of turgor pressure in oscillatory plant cell growth. *PLoS ONE* 6: 18549.
- Kumagai T, Saitoh TM, Sato Y, Takahashi H, Manfroi OJ, Morooka T, Kuraji K, Suzuki M, Yasunari T, Komatsu H. 2005. Annual water balance and seasonality of evapotranspiration in a Bornean tropical rainforest. *Agricultural and Forest Meteorology* 128: 81–92.
- Kunert N, Aparecido LMT, Wolff S, Higuchi N, Santos J, Araujo AC, Trumbore S. 2017. A revised hydrological model for the Central Amazon: the importance of emergent canopy trees in the forest water budget. *Agricultural and Forest Meteorology* 239: 47–57.

- Law BE, Falge E, Gu L, Baldocchi DD, Bakwin P, Berbigier P, Davis K, Dolman AJ, Falk M, Fuentes JD *et al.* 2002. Environmental controls over carbon dioxide and water vapor exchange of terrestrial vegetation. *Agricultural and Forest Meteorology* 113: 97–120.
- Lines ER, Zavala MA, Purves DW, Coomes DA. 2012. Predictable changes in aboveground allometry of trees along gradients of temperature, aridity and competition. *Global Ecology and Biogeography* 21: 1017–1028.
- Lion M, Kosugi Y, Takanashi S, Noguchi S, Itoh M, Katsuyama M, Matsuo N, Shamsuddin SA. 2017. Evapotranspiration and water source of a tropical rainforest in peninsular Malaysia. *Hydrological Processes* 31: 4338–4353.
- Liu H, Gleason SM, Hao G, Hua L, He P, Goldstein G, Ye Q. 2019. Hydraulic traits are coordinated with maximum plant height at the global scale. *Science Advances* 5: 1332.
- Lockhart JA. 1965. An analysis of irreversible plant cell elongation. *Journal of Theoretical Biology* 8: 264–275.
- Locosselli GM, Brien RJW, de Souza LM, Gloor M, Krotenthaler S, de Oliveira AA, Barichivich J, Anhof D, Ceccantini G, Schöngart J *et al.* 2020. Global tree-ring analysis reveals rapid decrease in tropical tree longevity with temperature. *Proceedings of the National Academy of Sciences, USA* 117: 33358–33364.
- López J, Way DA, Sadok W. 2021. Systemic effects of rising atmospheric vapor pressure deficit on plant physiology and productivity. *Global Change Biology* 27: 1704–1720.
- Mallick K, Trebs I, Boegh E, Giustarini L, Schlerf M, Hoffmann L, von Randow C, Kruijt B, Araújo A, Ehleringer JR *et al.* 2016. Canopy-scale biophysical controls of transpiration and evaporation in the Amazon Basin. *Hydrology and Earth System Sciences Discussions* 30: 1–50.
- Martin PH, Canham CD. 2020. Peaks in frequency, but not relative abundance, occur in the center of tree species distributions on climate gradients. *Ecosphere* 11: 3149.
- McDowell NG, Allen CD. 2015. Darcy's law predicts widespread forest mortality under climate warming. *Nature Climate Change* 5: 669–672.
- McJannet D. 2007a. Water balance of tropical rainforest canopies in north Queensland, Australia. *Hydrological Processes* 2274: 2267–2274.
- McJannet D. 2007b. Measurements of transpiration in four tropical rainforest types of north Queensland, Australia. *Hydrological Processes* 2274: 2267–2274.
- Moncrieff GR, Hickler T, Higgins SI. 2015. Intercontinental divergence in the climate envelope of major plant biomes. *Global Ecology and Biogeography* 24: 324–334.
- Monroe JG, Cai H, Des Marais DL, Grey Monroe J, Cai H, Des Marais DL. 2020. Trait plasticity and covariance along a continuous soil moisture gradient. *bioRxiv*. doi: 10.1101/2020.02.17.952853.
- Murphy HT, Bradford MG, Dalongeville A, Ford AJ, Metcalfe DJ. 2013. No evidence for long-term increases in biomass and stem density in the tropical rain forests of Australia. *Journal of Ecology* 101: 1589–1597.
- Niklas KJ. 2007. Maximum plant height and the biophysical factors that limit it. *Tree Physiology* 27: 433–440.
- Novick KA, Ficklin DL, Stoy PC, Williams CA, Bohrer G, Oishi AC, Papuga SA, Blanken PD, Noormets A, Sulman BN *et al.* 2016. The increasing importance of atmospheric demand for ecosystem water and carbon fluxes. *Nature Climate Change* 6: 1023–1027.
- Oishi AC, Hawthorne DA, Oren R. 2016. ScienceDirect Baseline: an open-source, interactive tool for processing sap flux data from thermal dissipation probes. *SoftwareX* 5: 139–143.
- Oliveira RS, Eller CB, Barros FDV, Hirota M, Brum M, Bittencourt P. 2021. Linking plant hydraulics and the fast–slow continuum to understand resilience to drought in tropical ecosystems. *New Phytologist* 230: 904–923.
- Olson ME, Anfodillo T, Rosell JA, Martínez-Méndez N, Rosell JA. 2020. Across climates and species, higher vapour pressure deficit is associated with wider vessels for plants of the same height. *Plant, Cell & Environment* 43: 3068–3080.
- Olson ME, Soriano D, Rosell JA, Anfodillo T, Donoghue MJ, Edwards EJ, León-Gómez C, Dawson T, Julio Camarero Martínez J, Castorena M *et al.* 2018. Plant height and hydraulic vulnerability to drought and cold. *Proceedings of the National Academy of Sciences, USA* 115: 7551–7556.
- Oren R, Sperry JS, Katul GG, Pataki DE, Ewers BE, Phillips N, Schäfer KVR. 1999. Survey and synthesis of intra- and interspecific variation in stomatal sensitivity to vapour pressure deficit. *Plant, Cell & Environment* 22: 1515–1526.
- Pereira L, Bittencourt PRL, Oliveira RS, Junior MBMM, Barros FV, Ribeiro RV, Mazzafera P, Pereira L, Bittencourt PRL, Oliveira RS *et al.* 2016. Plant pneumatics: stem air flow is related to embolism – new perspectives on methods in plant hydraulics. *New Phytologist* 211: 357–370.
- Peters JMR, López R, Nolf M, Hutley LB, Wardlaw T, Cernusak LA, Choat B. 2021. Living on the edge: a continental-scale assessment of forest vulnerability to drought. *Global Change Biology* 27: 3620–3641.
- Peters RL, Stepe K, Cuny HE, De Pauw DJW, Frank DC, Schaub M, Rathgeber CBK, Cabon A, Fonti P. 2021. Turgor – a limiting factor for radial growth in mature conifers along an elevational gradient. *New Phytologist* 229: 213–229.
- Phillips OL, Aragão LEOC, Lewis SL, Fisher JB, Lloyd J, López-González G, Malhi Y, Monteagudo A, Peacock J, Quesada C *et al.* 2009. Drought sensitivity of the Amazon Rainforest. *Science* 323: 1344–1347.
- Phillips OL, van der Heijden G, Lewis SL, López-González G, Aragão LE, Lloyd J, Malhi Y, Monteagudo A, Almeida S, Dávila EA *et al.* 2010. Drought-mortality relationships for tropical forests. *New Phytologist* 187: 631–646.
- Pommerening A, Muszta A. 2016. Relative plant growth revisited: Towards a mathematical standardisation of separate approaches. *Ecological Modelling* 320: 383–392.
- Potkay A, Hölttä T, Trugman AT, Fan Y. 2021. Turgor-limited predictions of tree growth, height and metabolic scaling over tree lifespans. *Tree Physiology* 42: 1–24.
- Rada F, Goldstein G, Azocar A, Meinzer F. 1985. Daily and seasonal osmotic changes in a tropical treeline species. *Journal of Experimental Botany* 36: 989–1000.
- Rosas T, Mencuccini M, Barba J, Cochard H, Saura-Mas S, Martínez-Vilalta J. 2019. Adjustments and coordination of hydraulic, leaf and stem traits along a water availability gradient. *New Phytologist* 223: 632–646.
- Rowland L, Ramírez-Valiente JA, Hartley IP, Mencuccini M. 2023. How woody plants adjust above- and below-ground traits in response to sustained drought. *New Phytologist* 239: 1173–1189.
- Sanchez-Martinez P, Martínez-Vilalta J, Dexter KG, Segovia RA, Mencuccini M. 2020. Adaptation and coordinated evolution of plant hydraulic traits. *Ecology Letters* 23: 1599–1610.
- Sanginés de Cárcer P, Vitasse Y, Peñuelas J, Jassby VEJ, Buttler A, Signarbioux C. 2018. Vapor–pressure deficit and extreme climatic variables limit tree growth. *Global Change Biology* 24: 1108–1122.
- Schiatti J, Emilio T, Rennó CD, Drucker DP, Costa FRC, Nogueira A, Baccaro FB, Figueiredo F, Castilho CV, Kinupp V *et al.* 2014. Vertical distance from drainage drives floristic composition changes in an Amazonian rainforest. *Plant Ecology and Diversity* 7: 241–253.
- Schlesinger WH, Jasechko S. 2014. Transpiration in the global water cycle. *Agricultural and Forest Meteorology* 189–190: 115–117.
- Schuldt B, Leuschner C, Horna V, Moser G, Köhler M, Van Straaten O, Barus H. 2011. Change in hydraulic properties and leaf traits in a tall rainforest tree species subjected to long-term throughfall exclusion in the perhumid tropics. *Biogeosciences* 8: 2179–2194.
- Sergent AS, Varela SA, Barigah TS, Badel E, Cochard H, Dalla-Salda G, Delzon S, Fernández ME, Guillemot J, Gyenge J *et al.* 2020. A comparison of five methods to assess embolism resistance in trees. *Forest Ecology and Management* 468: 118175.
- Silvertown J, Araya Y, Gowing D. 2015. Hydrological niches in terrestrial plant communities: a review. *Journal of Ecology* 103: 93–108.
- Smith MN, Taylor TC, van Haren J, Rosolem R, Restrepo-Coupe N, Adams J, Wu J, de Oliveira RC, da Silva R, de Araujo AC *et al.* 2020. Empirical evidence for resilience of tropical forest photosynthesis in a warmer world. *Nature Plants* 6: 1225–1230.
- Sperry JS, Love DM. 2015. What plant hydraulics can tell us about responses to climate-change droughts. *New Phytologist* 207: 14–27.
- Stegen JC, Swenson NG, Enquist BJ, White EP, Phillips OL, Jørgensen PM, Weiser MD, Monteagudo Mendoza A, Núñez VP. 2011. Variation in above-ground forest biomass across broad climatic gradients. *Global Ecology and Biogeography* 20: 744–754.
- Tan ZH, Zhao JF, Wang GZ, Chen MP, Yang LY, He CS, Restrepo-Coupe N, Peng SS, Liu XY, Humberto R *et al.* 2019. Surface conductance for

- evapotranspiration of tropical forests: calculations, variations, and controls. *Agricultural and Forest Meteorology* 275: 317–328.
- Tang X, Li H, Desai AR, Nagy Z, Luo J, Kolb TE, Oliosio A, Xu X, Yao L, Kutsch W *et al.* 2014. How is water-use efficiency of terrestrial ecosystems distributed and changing on Earth? *Scientific Reports* 4: 1–11.
- Tavares JV, Oliveira RS, Mencuccini M, Signori-Müller C, Pereira L, Diniz FC, Gilpin M, Marca Zevallos MJ, Salas Yupayccana CA, Acosta M *et al.* 2023. Basin-wide variation in tree hydraulic safety margins predicts the carbon balance of Amazon forests. *Nature* 617: 111–117.
- Terry L, Calders K, Bartholomeus H, Bartolo RE, Brede B, D'hont B, Disney M, Herold M, Lau A, Shenkin A *et al.* 2022. Quantifying tropical forest structure through terrestrial and UAV laser scanning fusion in Australian rainforests. *Remote Sensing of Environment* 271: 112912.
- Tng DYP, Apgaua DMG, Ishida YF, Mencuccini M, Lloyd J, Laurance WF, Laurance SGW. 2018. Rainforest trees respond to drought by modifying their hydraulic architecture. *Ecology and Evolution* 8: 12479–12491.
- Trueba S, Pouteau R, Lens F, Feild TS, Isnard S, Olson ME, Delzon S. 2017. Vulnerability to xylem embolism as a major correlate of the environmental distribution of rain forest species on a tropical Island. *Plant, Cell & Environment* 40: 277–289.
- Trugman AT, Anderegg LDL, Shaw JD, Anderegg WRL. 2020. Trait velocities reveal that mortality has driven widespread coordinated shifts in forest hydraulic trait composition. *Proceedings of the National Academy of Sciences, USA* 117: 8532–8538.
- Tsuji S, Nakashizuka T, Kuraji K, Kume A, Hanba YT. 2020. Sensitivity of stomatal conductance to vapor pressure deficit and its dependence on leaf water relations and wood anatomy in nine canopy tree species in a Malaysian wet tropical rainforest. *Trees – Structure and Function* 34: 1299–1311.
- Ward EJ, Domec JC, King J, Sun G, McNulty S, Noormets A, Ward EJ. 2017. An open source software for processing sap flux data from thermal dissipation probes. *Trees* 31: 1737–1742.
- Wei ZZ, Yoshimura K, Wang L, Miralles DG, Jasechko S, Lee X. 2017. Revisiting the contribution of transpiration to global terrestrial evapotranspiration. *Geophysical Research Letters* 44: 2792–2801.
- Whitehead D, Edwards WRN, Jarvis PG. 1984. Conducting sapwood area, foliage area, and permeability in mature trees of *Picea sitchensis* and *Pinus contorta*. *Canadian Journal of Forest Research* 14: 940–947.
- Woodruff DR, Bond BJ, Meinzer FC. 2004. Does turgor limit growth in tall trees? *Plant, Cell & Environment* 27: 229–236.
- Yuan W, Zheng Y, Piao S, Ciais P, Lombardozi D, Wang Y, Ryu Y, Chen G, Dong W, Hu Z *et al.* 2019. Increased atmospheric vapor pressure deficit reduces global vegetation growth. *Science Advances* 5: 1–13.
- Zeri M, Sá LDA, Manzi AO, Araújo AC, Aguiar RG, Von Randow C, Sampaio G, Cardoso FL, Nobre CA. 2014. Variability of carbon and water fluxes following climate extremes over a tropical forest in southwestern Amazonia. *PLoS ONE* 9: e88130.
- Zhang K, Kimball JS, Nemani RR, Running SW, Hong Y, Gourley JJ, Yu Z. 2015. Vegetation greening and climate change promote multidecadal rises of global land evapotranspiration. *Scientific Reports* 5: 1–9.
- Zhang X, Chhin S, Fu L, Lu L, Duan A, Zhang J. 2019. Climate-sensitive tree height–diameter allometry for Chinese fir in southern China. *Forestry: An International Journal of Forest Research* 92: 167–176.
- Zhang Y, Lamarque LJ, Torres-Ruiz JM, Schuldt B, Karimi Z, Li S, Qin D-WW, Bittencourt P, Burlett R, Cao K-FF *et al.* 2018. Testing the plant pneumatic method to estimate xylem embolism resistance in stems of temperate trees. *Tree Physiology* 38: 1–10.
- Zhao H, Li Y, Liao S, Jiang Z, Cai J. 2023. Further test of pneumatic method in constructing vulnerability curves using six tree species with contrasting xylem anatomy. *Forests* 14: 293.

Supporting Information

Additional Supporting Information may be found online in the Supporting Information section at the end of the article.

Fig. S1 Soil water potential monthly means of Cow Bay and Robson Creek.

Fig. S2 Comparison of the long-term meteorological conditions with the conditions during the study at Cow Bay and Robson Creek.

Fig. S3 Per cent air discharged curves from Cow Bay and Robson Creek.

Fig. S4 Predicting canopy water potentials using whole-tree hydraulic conductance, sap flux and soil water potential.

Fig. S5 Hydraulic safety margins based on measured vs modelled minimum canopy water potentials.

Methods S1 Pneumatic branch vulnerability curves.

Please note: Wiley is not responsible for the content or functionality of any Supporting Information supplied by the authors. Any queries (other than missing material) should be directed to the *New Phytologist* Central Office.